Nanoscale

PAPER

View Article Online
View Journal | View Issue

Check for updates

Cite this: *Nanoscale*, 2023, **15**, 17464

Ruptured organosilica nanocapsules immobilized acetylcholinesterase coupled with MnO_2 nanozyme for screening inhibitors from *Inula macrophylla*†

Jia Liu,[a,c] Wei Ha,[a] Eshbakova Komila Alibekovna,[b] Rui Ma[a] and Yan-Ping Shi *[a]

Received 11th August 2023,
Accepted 6th October 2023

DOI: 10.1039/d3nr04025a

rsc.li/nanoscale

Abnormal expression of acetylcholinesterase (AChE) causes Alzheimer's disease (AD). Inhibiting AChE is a common strategy for reducing the degradation of neurotransmitter acetylcholine, in order to treat early-stage AD. Therefore, it is crucial to screen and explore AChE inhibitors which are safer and cause fewer side effects. Our research is focused on establishing a platform of ruptured organosilica nanocapsules (RONs) immobilized AChE coupled with an MnO_2–OPD colorimetric assay, which could monitor AChE activity and screen AChE inhibitors. The fabricated RONs immobilized AChE possessed excellent pH and thermal stability. Huperzine A was introduced into the established platform to evaluate the inhibition kinetics of the immobilized AChE, which promoted its application in the screening of AChE inhibitors. The satisfactory results of enzyme inhibition kinetics proved the feasibility and applicability of the established method. Thus, the proposed platform was applied to screen AChE inhibitors from 14 compounds isolated from *Inula macrophylla*, and β-cyclocostunolide (compound **4**) demonstrated the best AChE inhibitory activity among these compounds. This work confirms the existence of chemical components that inhibit AChE activity in *Inula macrophylla*, and provides a new idea for the application of immobilized enzyme–nanozyme in the field of enzyme inhibitor screening.

Open Access Article. Published on 11 2566. Downloaded on 24/7/2567 16:33:59.
This article is licensed under a Creative Commons Attribution-NonCommercial 3.0 Unported Licence.

1. Introduction

Acetylcholinesterase (AChE), a cholinesterase present in the nervous system, plays the role of regulating nerve signal transmission.[1,2] Abnormal concentration of neurotransmitter acetylcholine is associated with AChE, which catalyzes the hydrolysis reaction of acetylcholine to choline.[3] Accordingly, a low level of acetylcholine could cause neurodegenerative diseases, such as Alzheimer's disease.[4,5] Inhibiting AChE activity, which is regarded as an effective strategy for treating Alzheimer's disease, could promote the accumulation of acetylcholine.[6–8] Consequently, monitoring AChE activity and exploring AChE inhibitors is significant for early disease diagnosis and drug discovery.

Numerous strategies have been developed for detecting AChE activity, including a fluorescent method,[9] an electrochemical assay[10] and a chemiluminescent method.[11] Conventional strategies still suffer several drawbacks such as false-positive effects, being time-consuming and requiring sophisticated equipment, which limit the application of these strategies. Moreover, a colorimetric assay is highlighted for its on-site visual inspection, due to its simplicity, economy, speed, and direct quantification.[12,13] An *O*-phenylenediamine (OPD)-based colorimetric assay is employed as an effective approach to quantify analytes in the absence of expensive reagents or complicated operation. Accordingly, colorless OPD used as a chromogenic substrate, could be oxidated into its yellow-colored oxidized product 2.3-diaminophenazine (ox OPD) by nanozymes.[14] Nanozymes are nanomaterials with enzyme-mimicking activity, possessing the unique properties of low cost, excellent stability, high activity, easy storage, simple recyclability and mass production. Considering the above advantages, nanozymes have been applied to enzyme inhibitor screening. For example, Su *et al.* employed MIL-101 (Cr)@PB prepared by an *in situ* growth synthetic strategy as a novel peroxidase mimicking material, and a colorimetric platform for screening xanthine oxidase inhibitors was constructed.[15] This also elucidated the promising application of

[a]*CAS Key Laboratory of Chemistry of Northwestern Plant Resources, Key Laboratory for Natural Medicines of Gansu Province, Lanzhou Institute of Chemical Physics, Chinese Academy of Sciences (CAS), Lanzhou 730000, P. R. China.*
E-mail: shiyp@licp.cas.cn
[b]*S. Yu. Yunusov Institute of the Chemistry of Plant Substances, Academy of Sciences of the Republic of Uzbekistan, Uzbekistan*
[c]*University of Chinese Academy of Sciences, Beijing 100049, P. R. China*
† Electronic supplementary information (ESI) available. See DOI: https://doi.org/10.1039/d3nr04025a

This journal is © The Royal Society of Chemistry 2023

Open Access Article. Published on 11 2566. Downloaded on 24/7/2567 16:33:59.
This article is licensed under a Creative Commons Attribution-NonCommercial 3.0 Unported Licence.

nanozymes in drug screening. Additionally, numerous nanomaterials, including Au,[16] Pt,[17] Fe_2O_3 [18] and MnO_2,[19] have been found to exhibit oxidase-like activity, which could serve as emerging alternatives to natural enzymes.[20,21] MnO_2 nanosheets, as a type of two-dimensional nanomaterial, have attracted considerable attention due to their simple preparation and excellent water solubility.[22–24] Thus, MnO_2 nanosheets with low toxicity could serve as an oxidizer in an OPD-based colorimetric assay.

Immobilization of an enzyme is an effective tool to satisfy the demands of reuse, easy separation from the reaction medium and better tolerance to even harsh reaction conditions.[25,26] The targeted benefits facilitate the application of an immobilized enzyme. Capillary electrophoresis is an effective tool to quantitatively detect the enzymatic reaction product, due to its high efficiency of separation and analysis, and low consumption of sample and solvent.[27,28]

Inspired by the above, we combined the easy separation of an AChE strategy immobilization with the convenience of an MnO_2–OPD colorimetric assay, a strategy that has rarely been reported. Moreover, the integration of these two methodologies not only realizes the detection of AChE activity, but also achieves the screening of AChE inhibitors. The reaction principle of screening AChE inhibitors is as follows (Fig. 1). Thiocholine (TCh), an AChE-catalyzed hydrolysate for acetylthiocholine, could trigger the decomposition of MnO_2 nanosheets to generate Mn^{2+}. The remaining MnO_2 nanosheets could oxidize colorless OPD into the yellow-colored product ox OPD with a characteristic absorption at 420 nm. By quantitative determination of absorption peaks with capillary electrophoresis, AChE activity could be evaluated. When an AChE inhibitor is introduced, a reduction in TCh and an increase in absorption of ox OPD could occur. Thus, this platform could open up a promising avenue for analysis of AChE activity based on the immobilization of enzyme and nanozyme.

Herein, ruptured organosilica nanocapsules (RONs) were prepared by the hard-templating method for AChE immobilization.[29–31] Cracks and openings on the surface of RONs could promote the immobilization of AChE on the interior and exterior of RONs *via* electrostatic interactions. Additionally, the nanocapsule wall acted as a barrier, protecting the interior from interference by the external environment and leaching.[32] Combining the established RONs immobilized AChE with an MnO_2–OPD colorimetric assay, a platform was fabricated to monitor AChE activity and screen AChE inhibitors.

2. Experimental

2.1. Chemicals

Manganese chloride tetrahydrate ($MnCl_2{\cdot}4H_2O$), sodium dihydrogen phosphate (NaH_2PO_4), disodium hydrogen phosphate (Na_2HPO_4), sodium tetraborate decahydrate ($Na_2B_4O_7{\cdot}10H_2O$), acetic acid (HAc), hydrochloric acid (HCl) and sodium hydroxide (NaOH) were obtained from Tianjin Kermel Chemical Reagent Co., Ltd (Tianjin, China). 2-Methylimidazole (2-MeIM), ethylene diamine tetraacetic acid (EDTA) and tetramethylammonium hydroxide were purchased from Beijing J&K Chemical Technology Co., Ltd (Beijing, China). Methanol was purchased from Li'anlong Bohua Pharmaceutical Chemical Co., Ltd (Tianjin, China). Tetraethyl orthosilicate (TEOS) and huperzine A were acquired from Macklin Biochemical Co., Ltd (Shanghai, China). (3-Aminopropyl)triethoxysilane (APTES) and zinc nitrate hexahydrate ($Zn(NO_3)_2{\cdot}6H_2O$) were purchased from Aladdin Bio-Chem Technology Co., Ltd (Shanghai, China). Hydrogen peroxide (H_2O_2, 30 wt%) and sodium acetate (NaAc) were obtained from Xilong Scientific Co., Ltd (Guangdong, China). Acetylcholinesterase (AChE) from *Electrophorus electricus* (electric eel) and acetylthiocholine chloride (AThCh) were purchased from Sigma Chemical Co., Ltd (St Louis, MO, USA). AChE (0.8 mg mL^{-1}), AThCh (5 mM) and huperzine A (1 mM) stock solutions were prepared in phosphate buffer (30 mM, pH 5.0) and stored at 4 °C before use.

2.2. CE conditions

The reaction product was separated and detected with an Agilent 7100 capillary electrophoresis system equipped with a diode array detector (DAD). An uncoated fused silica capillary (Yongnian Ruifeng Chromatographic Device Co., Ltd, Hebei, China) with a length of 33 cm (24.5 cm from the detection window) and an inner diameter of 50 μm was used as the separation medium in CE analysis. A voltage of 28 kV and a pressure of 25 mbar were applied, and the samples were separated and analyzed at a wavelength of 420 nm. Before the beginning of the daily experiment, the capillary was rinsed with 0.1

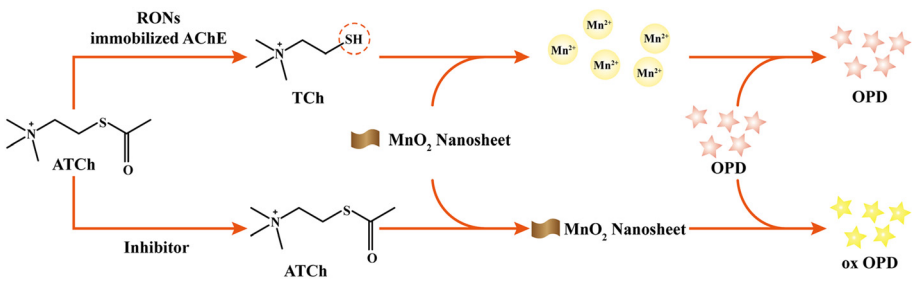

Fig. 1 Schematic of the assay of RONs immobilized AChE coupled with MnO_2 nanosheets for its inhibitor screening.

Open Access Article. Published on 11 2566. Downloaded on 24/7/2567 16:33:59.
This article is licensed under a Creative Commons Attribution-NonCommercial 3.0 Unported Licence.

M NaOH for 15 min, ultrapure water for 20 min and 10 mM $Na_2B_4O_7{\cdot}10H_2O$ (pH = 9.0) for 10 min to initialize the capillary. After the experiment, the capillary was rinsed with 0.1 M NaOH for 15 min and ultrapure water for 20 min to keep the inner wall of the capillary clean.

2.3. Characterization

Transmission electron microscopy (TEM) was collected using a Tecnai-G2-F30 (FEI, USA); scanning electron microscopy (SEM) was performed using an SU 8020 (JSM-5601LV, JEOL); Fourier transform infrared (FT-IR) spectra were measured using a Nexus 870 (Nicolet, USA); X-ray diffraction was analyzed with a Smartlab-SE (Japan); Brunauer–Emmett–Teller (BET) measurements were made using an ASAP 2020M (Micromeritics, USA); the zeta potential of the materials was measured by dynamic light scattering (Malvern, ZEN 3600, Malvern Instruments, UK); the Raman spectrum was obtained with a LabRAM HR Evolution (HORIBA Jobin Yvon S.A.S., French); X-ray photoelectron spectroscopy (XPS) analysis was carried out using an ESCALAB 250Xi X-ray photoelectron spectrometer (Thermo Fisher scientific, USA).

2.4. Preparation of ruptured organosilica nanocapsules (RONs) immobilized AChE

An aqueous solution of $Zn(NO_3)_2{\cdot}6H_2O$ (24 mL, 0.14 mM) was prepared and quickly poured into an aqueous solution of 2-methylimidazole (40 mL, 3 mM). Subsequently, the obtained solution was magnetically stirred for 15 min and the resulting solution was centrifuged for 10 min and washed with deionized water several times. ZIF-8 was eventually acquired.

The synthesized ZIF-8 (60 mg) was completely dispersed in 9 mL of deionized water and sonicated for 5 min. Immediately, 130 μL of TEOS was added into the above suspension and vigorously shaken for 30 min. Then, 21 μL of APTES was added to make a final concentration of 9.97 mM. The mixture was shaken for 4 h, centrifuged for 10 min and washed three times with deionized water. The obtained product was named ZIF-8/RONs. Finally, the RONs were acquired by treating ZIF-8/RONs with EDTA (50 mM) to remove the template.

The as-synthesized RONs were dispersed in phosphate buffer (30 mM, pH = 5) to obtain a homogeneous suspension. Then, an AChE solution (0.5 mg mL^{-1}) was added dropwise into the above suspension and the mixture was shaken for 3 h. After that, the sample was centrifuged and washed with deionized water and RONs immobilized AChE was acquired. The preparation process of RONs immobilized AChE is displayed in Fig. 2.

2.5. Assay of RONs immobilized AChE activity

50 μL of AThCh (5 mM) was mixed with 20 μL of RONs immobilized AChE and incubated in a 35 °C water bath for 15 min. Then, 50 μL of MnO_2 nanosheets was added into the mixture and reacted for 10 min, followed by the addition of NaAc buffer (200 mM, pH = 4) and OPD (50 μL). After a reaction time of 15 min, the mixture was centrifuged and the produced yellow-colored ox OPD was collected, and analyzed by CE at a wavelength of 420 nm. Each experiment was repeated three times.

The kinetic parameters of RONs immobilized AChE was determined by incubating with a series of different concentrations of AThCh (1 mM to 5 mM) and the enzyme activity was evaluated by the section of assay of RONs immobilized AChE activity. Kinetic analysis was performed by monitoring the absorbance change of the ox OPD at 420 nm. The Michaelis constant (K_m) was calculated with the Michaelis–Menten equation:[33]

$$\frac{1}{v} = \left(\frac{K_m}{V_{max}}\right)\left(\frac{1}{[S]}\right) + \frac{1}{V_{max}} \quad (1)$$

where v and V_{max} represent the initial and maximal reaction velocity, respectively, and S is the concentration of AThCh.

P_0 and P are the peak areas of the product (yellow-colored ox OPD) in the MnO_2–OPD system in the absence and presence of RONs immobilized AChE. Thus, v in the Michaelis–Menten equation was represented by $\Delta P = P_0 - P$.

2.6. Assay of the oxidase-like activity of MnO_2 nanosheets

The oxidase-like activity of MnO_2 nanosheets was assayed by choosing OPD as the substrate. Unlike the RONs immobilized AChE activity assay, a fixed concentration of AThCh (5 mM) and various concentrations of OPD (0.8 mM to 4 mM) were added in the assay of MnO_2 nanozyme activity. Here v in the Michaelis–Menten equation was represented by P.

2.7. Evaluation of the inhibitory effect of huperzine A

Huperzine A, a traditional AChE inhibitor, was employed as a model inhibitor to evaluate the inhibitory activity for the RONs immobilized AChE–MnO_2–OPD system. Different concentrations of huperzine A (20 μL) and RONs immobilized AChE (20 μL) were mixed at 35 °C for 20 min. Then, AThCh (5 mM, 50 μL) was added and incubated at 35 °C for 15 min. Subsequently, 50 μL of MnO_2 nanosheets was added into the

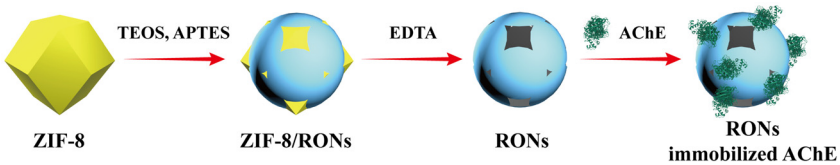

Fig. 2 The preparation process of RONs immobilized AChE.

This journal is © The Royal Society of Chemistry 2023

Open Access Article. Published on 11 2566. Downloaded on 24/7/2567 16:33:59.
This article is licensed under a Creative Commons Attribution-NonCommercial 3.0 Unported Licence.

mixture and reacted for 10 min, followed by the addition of NaAc buffer (200 mM, pH = 4) and OPD (50 μL). After a reaction time of 15 min, the mixture was centrifuged and the produced yellow-colored ox OPD was collected and analyzed by CE at a wavelength of 420 nm. Each experiment was repeated three times. The inhibition (IE%) was used as the basis of analysis of huperzine A for the RONs immobilized AChE–MnO_2–OPD system. IE% was analyzed with the following eqn (2):

$$\text{IE}\ (\%) = (P_{\text{inhibitor}} - P_{\text{no inhibitor}})/(P_0 - P_{\text{no inhibitor}}) \times 100\% \quad (2)$$

where $P_{\text{inhibitor}}$ and $P_{\text{no inhibitor}}$ represent the peak areas of the product (yellow-colored ox OPD) in the RONs immobilized AChE–MnO_2–OPD-huperzine A system and RONs immobilized AChE–MnO_2–OPD system, respectively. P_0 refers to the peak areas of the product (yellow-colored ox OPD) in the MnO_2–OPD system without RONs immobilized AChE and huperzine A.

2.8. Procedures for screening inhibitors from *Inula macrophylla*

2.8.1. Preparation of *Inula macrophylla*. *Inula macrophylla* from Uzbekistan was provided and authenticated by Professor K. A. Eshbakova.

At room temperature, the dried rhizome of *Inula macrophylla* (10 kg) was soaked in ethanol (18 L) 5 times, for 24 h each time. The ethanol extract was dispersed in water and extracted with ethyl acetate. The extract was concentrated under reduced pressure to obtain 307 g of ethyl acetate extract. The ethyl acetate extract was eluted with a normal-phase silica gel column (200–300 mesh) and dichloromethane/methanol system (1 : 0 to 0 : 1, v/v) to obtain five main fractions A–E. Fraction B (25 g) was fractionated by a medium-pressure liquid-phase methanol/water system (from 20/80 to 100/0, v/v) to obtain six subfractions B_1–B_6. Fraction B_3 was eluted on silica gel (200–300 mesh) and Sephadex LH-20, and purified with HPLC (CH_3CN–H_2O from 40 : 60 to 60 : 40, v/v) to obtain compounds **1** and **2**. Fraction B_4 was eluted with Sephadex LH-20 and purified with HPLC (CH_3OH–H_2O from 40 : 60 to 60 : 40, v/v) to obtain compounds **3**, **4** and **5**. Fraction C (15 g) was eluted in a medium-pressure liquid-phase methanol/water system (from 20/80 to 100/0, v/v) to obtain eight subfractions (C_1–C_8). Fraction C_2 was eluted on normal-phase silica gel (200–300 mesh) and purified with HPLC to obtain compounds **6**, **7** and **8**. Fraction C_3 was eluted with Sephadex LH-20 and prepared with multiple HPLC to obtain **9**, **10**, **11**, **12**, **13** and **14**.

The phytochemistry of the extracts from the rhizomes of *Inula macrophylla* was studied, and the structures of 14 compounds were identified as macrophyllilactone A (compound **1**), (+)-costunolide (compound **2**), alloalantolactone (compound **3**), β-cyclocostunolide (compound **4**), isoalantolactone (compound **5**), (−)-12-hydroxyl-1,3,11(13)-elemene (compound **6**), 3-oxo-4,11-dien-12,8β-eudesmanolides (compound **7**), 3-oxo-7,11α,8β-4-ene-12,8-eudesmanolides (compound **8**), (4*R*,5*S*,10*S*)-5-hydroxy-11,12,13-trinitro-6-en-8-one (compound **9**), 10-isobutyryloxy-8,9-didehydrothymol isobutyrate (compound **10**), 5α,6α-epoxyeudesm-12,8β-lactone (compound **11**), 8,10-dihydroxy-9-isobutyryloxythymol (compound **12**), reynosin (compound **13**) and macrophyllilactone E (compound **14**). The structures of the compounds in *Inula macrophylla* are shown in Fig. S1.†

2.8.2. Screening inhibitors from *Inula macrophylla*. The established RONs immobilized AChE–MnO_2–OPD system was applied to screen AChE inhibitors from *Inula macrophylla*. By measuring the peak areas of the obtained product ox OPD, which was obtained by incubating RONs immobilized AChE with *Inula macrophylla* extract or compound, substrate AThCh, MnO_2 and OPD, thereby evaluating the inhibitory effect of the *Inula macrophylla* extract and compound. The screening process was described in section 2.7.

3. Results and discussion

3.1. Characterization of the materials

FT-IR spectra of ZIF-8, ZIF-8/RONs and RONs are presented in Fig. 3a. For ZIF-8, the band at 1570 cm^{-1} corresponds to the C–N stretching vibration.[34] The bands at 3182 cm^{-1} and 2927 cm^{-1} were attributed to the characteristic absorption of imidazole.[35] For ZIF-8/RONs, all the above-mentioned bands were observed, but the band intensities were weakened. In addition, the band at 1058 cm^{-1} was significantly enhanced, which could be assigned to the Si–O–Si stretching vibrations. For RONs, the bands of Si–O–Si stretching vibrations still existed, and the bands of ZIF-8 were weakly observed, due to the incomplete removal of ZIF-8.

Crystalline structures of ZIF-8, ZIF-8/RONs and RONs were characterized by XRD patterns. As shown in Fig. 3b, the characteristic peaks of ZIF-8 at 7.4°, 12.79° and 18.1° are very consistent with the simulated patterns for the crystal structure of ZIF-8.[36] For ZIF-8/RONs, the above characteristic peaks were weakened, which demonstrated the successful coating with organosilica. In the RONs sample, the weak presence of characteristic peaks for ZIF-8 could still be observed, indicating the incomplete removal of ZIF-8.

Nitrogen adsorption–desorption analysis of ZIF-8/RONs and RONs was conducted to determine the surface area (Fig. 3c). The RONs exhibited a Brunauer–Emmett–Teller (BET) surface area of 747.9 $m^2\ g^{-1}$, about 2.5-fold higher than that of ZIF-8/RONs (298.5 $m^2\ g^{-1}$). In addition, the pore size distribution of ZIF-8/RONs and RONs was calculated by the Barrett–Joyner–Halenda method, as displayed in Fig. 3d. The pore sizes of the two samples were determined as mesoporous with average diameters of 23.1 nm and 12.0 nm, respectively. Based on these results, the larger surface of RONs for AChE immobilization could be verified.

The zeta potentials of various materials are illustrated in Fig. 4. After coating with organosilica, the zeta potential of the material changes from positive to negative. After etching ZIF-8, a negatively charged sample was obtained, suggesting the successful preparation of RONs. This further laid the foundation for AChE immobilization in the following experiment, in

Open Access Article. Published on 11 2566. Downloaded on 24/7/2567 16:33:59.
This article is licensed under a Creative Commons Attribution-NonCommercial 3.0 Unported Licence.

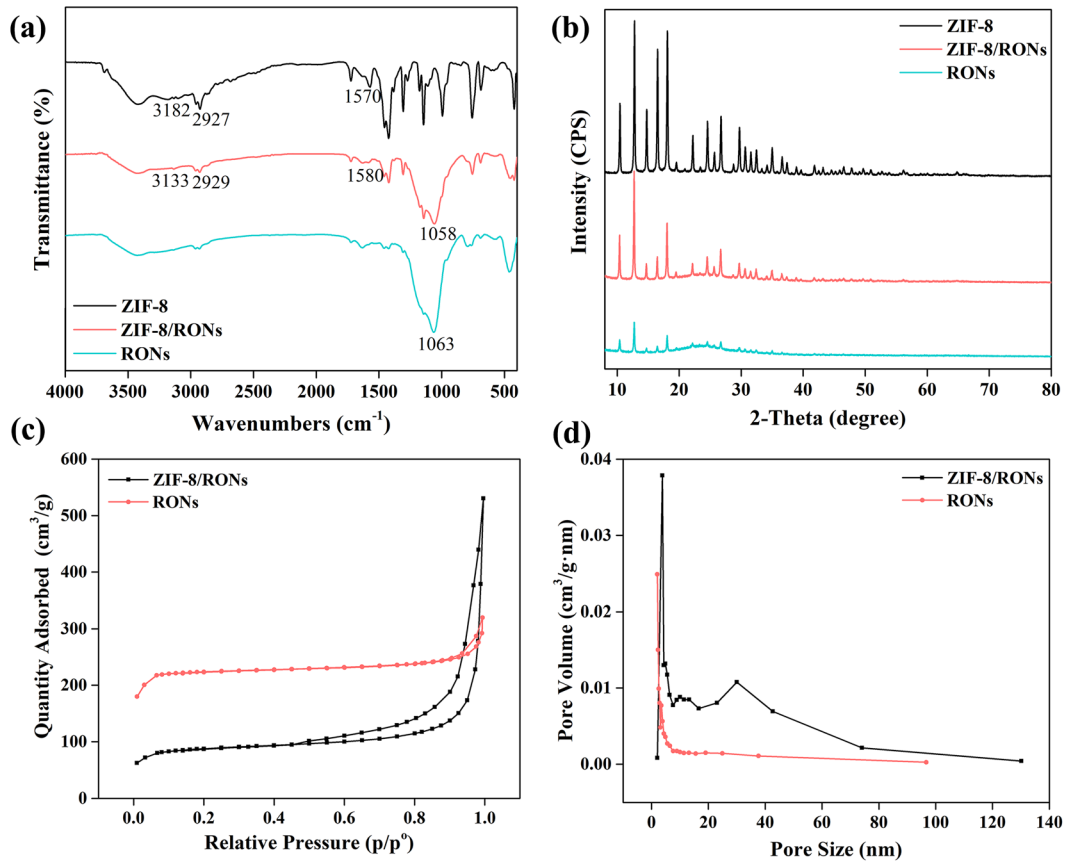

Fig. 3 (a) FT-IR spectra, (b) XRD curves, (c) N_2 extraction–desorption isotherms, (d) pore size of ZIF-8/RONs and RONs.

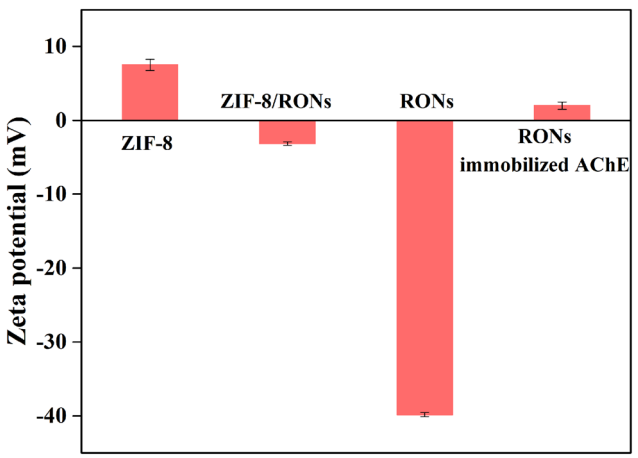

Fig. 4 Zeta potential of ZIF-8, ZIF-8/RONs, RONs and RONs immobilized AChE.

which positively charged AChE was immobilized on the negatively charged RONs through electrostatic interactions.

The SEM images and TEM images of ZIF-8, ZIF-8/RONs and RONs are presented in Fig. 5. The TEM image of ZIF-8 (Fig. 5d) shows a polygonal structure. After co-condensation between TEOS and APTES, a coating of organosilica was formed on ZIF-8 and ZIF-8/RONs were formed (Fig. 5b).[37] When the synthesized sample was treated with EDTA, cracks and openings appeared on the surface of ZIF-8/RONs, as shown in Fig. 5c and f. This phenomenon could be ascribed to the removal of the template.

The MnO_2 nanosheets were systematically characterized by TEM, Raman spectroscopy and XPS. The MnO_2 nanosheets showed a large sheet-like morphology and a typical two-dimensional structure, indicating that the nanostructures provide a large surface area and sufficient surface-active sites for the reaction with OPD (Fig. 6a). In the Raman spectrum, MnO_2 nanosheets presented a peak located at 549 cm^{-1}, corresponding to the Mn–O vibration (Fig. 6b). The XPS of the MnO_2 nanosheets displayed two peaks centered at 641.9 eV and 653.3 eV, belonging to $Mn_{2p3/2}$ and $Mn_{2p1/2}$, respectively (Fig. 6c).[38] All the characterizations verified the successful synthesis of MnO_2 nanosheets.

3.2. pH, thermal stability of RONs immobilized AChE and MnO_2 nanozyme

Immobilization parameters and reaction parameters of RONs immobilized AChE, including immobilization pH, immobilization time, concentration of immobilized AChE, enzymatic reaction time and enzymatic reaction temperature, were systematically optimized (Fig. S2†). Optimization of the chromogenic reaction of RONs immobilized AChE with OPD is shown in Fig. S3.†

This journal is © The Royal Society of Chemistry 2023

Open Access Article. Published on 11 2566. Downloaded on 24/7/2567 16:33:59.
This article is licensed under a Creative Commons Attribution-NonCommercial 3.0 Unported Licence.

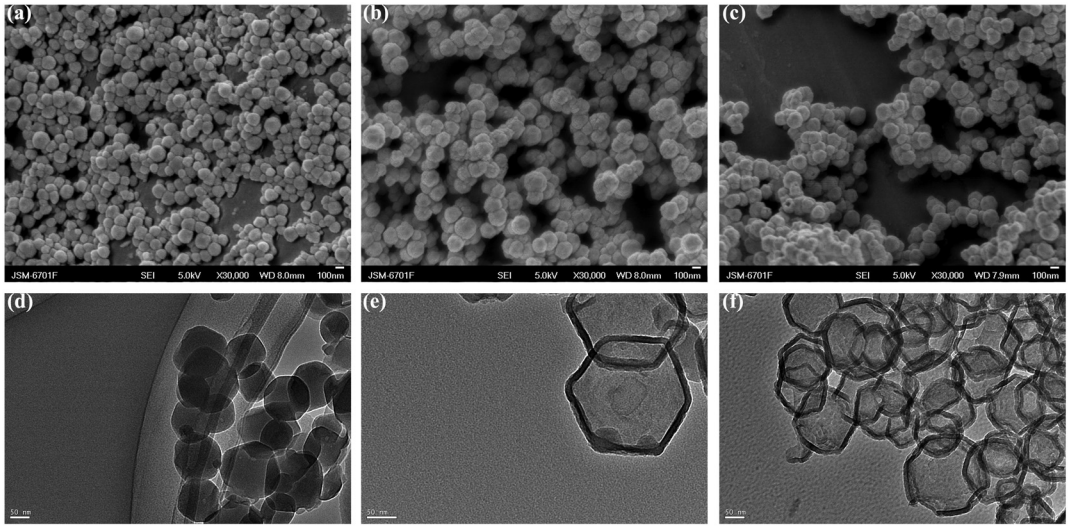

Fig. 5 SEM images of (a) ZIF-8, (b) ZIF-8/RONs, (c) RONs and TEM image of (d) ZIF-8, (e) ZIF-8/RONs, (f) RONs.

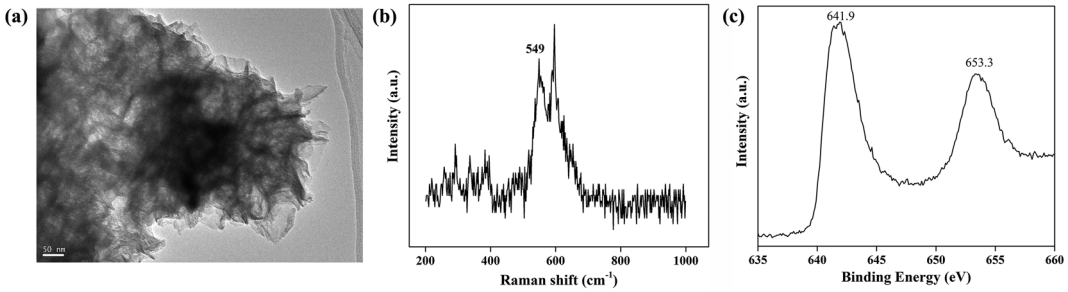

Fig. 6 (a) TEM image, (b) Raman spectrum and (c) XPS of MnO_2 nanosheets.

The pH and thermal stability of RONs immobilized AChE and MnO_2 nanozyme were investigated, respectively. The pH stability of RONs immobilized AChE and MnO_2 nanozyme were investigated by measuring the residual activities, after an incubation time of 1 h in different pH buffers (3, 4, 5, 6, 7, 8). For pH stability (Fig. 7a), RONs immobilized AChE and MnO_2 nanozyme could maintain high activity in the pH range of 3–8. The thermal stability of RONs immobilized AChE and MnO_2 nanozyme was evaluated by measuring the residual activities, after incubating for 1 h in a water bath at different temperatures (25, 35, 45, 55, 65 °C). The buffer used was PB buffer (pH 3–8). For thermal stability (Fig. 7b), RONs immobilized AChE and MnO_2 nanozyme could maintain relative activity of more than 90% within 35–45 °C and still maintain more than 60% of the original activity within 35–65 °C.

3.3. Enzyme kinetics analysis

K_m is regarded as a significant parameter for the Michaelis–Menten equation, which is associated with the affinity of an enzyme for a substrate. The K_m value of RONs immobilized AChE was determined as 0.49 mM (Fig. 8a). As another crucial parameter for evaluating the catalytic rate, V_{max} was 63.29 mM min^{-1}. The K_m and V_{max} values of MnO_2 nanozymes were 2.93 mM and 140.33 mM min^{-1}, respectively (Fig. 8b), which were superior to those of some natural enzymes and nanozymes.[39] The results showed that MnO_2 nanozyme had strong affinity and excellent catalytic rate for substrates, and may be an ideal substitute for oxidase.

In the presence of different concentrations of huperzine A (10, 30, 70 μM), three Lineweaver–Burk plots of RONs immobilized AChE were presented and intersected in the second quadrant (Fig. 9). With an increase in huperzine A concentration, the horizontal axis intercept value ($-1/K_m$) decreased and the vertical axis intercept value ($1/V_{max}$) increased, indicating that huperzine A had mixed competitive and non-competitive inhibition behavior.

Taking advantage of the excellent performance of the RONs immobilized AChE–MnO_2–OPD system, the proposed platform was further developed by investigating its potential application in detecting the AChE inhibitor, huperzine A. Huperzine A is a well-known inhibitor that could efficiently inhibit the hydrolysis of AChE.[40] When huperzine A was added into the RONs immobilized AChE–MnO_2–OPD system, the enzyme hydrolysis reaction was obviously suppressed and less TCh was generated,

Open Access Article. Published on 11 2566. Downloaded on 24/7/2567 16:33:59.
This article is licensed under a Creative Commons Attribution-NonCommercial 3.0 Unported Licence.

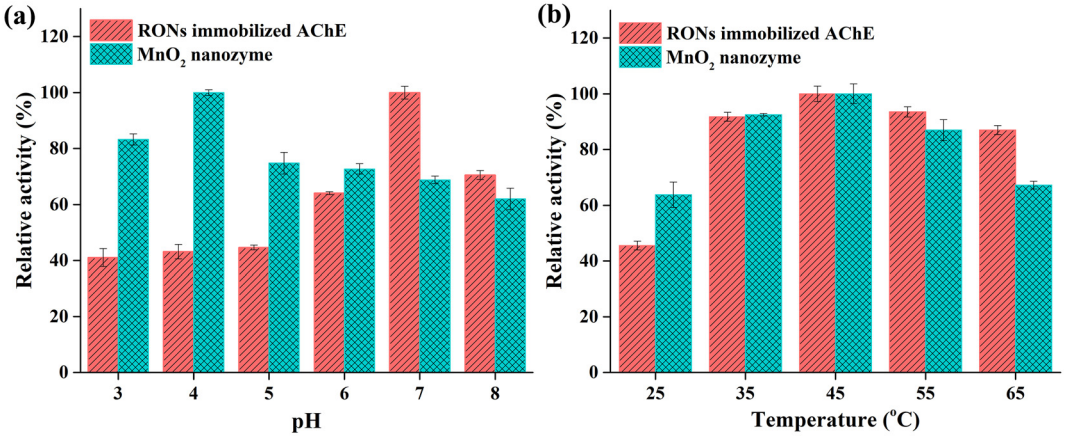

Fig. 7 (a) pH stability and (b) thermal stability of RONs immobilized AChE and MnO_2 nanozyme.

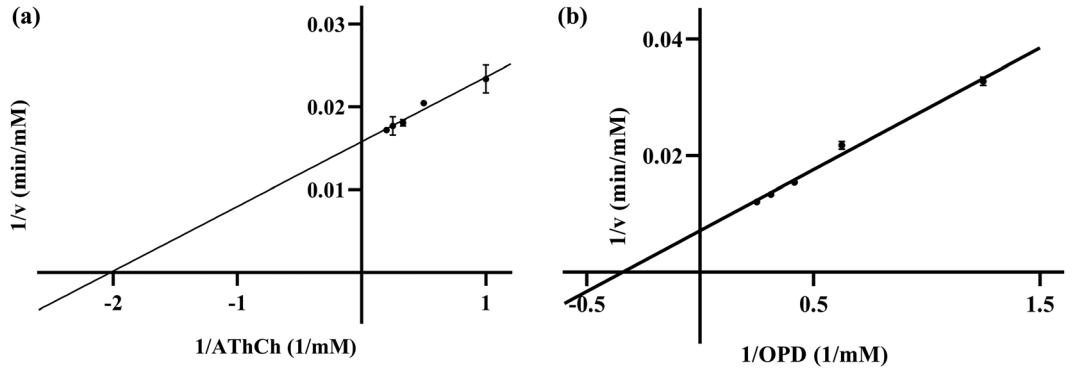

Fig. 8 Lineweaver–Burk plots of (a) RONs immobilized AChE and (b) MnO_2 nanozyme.

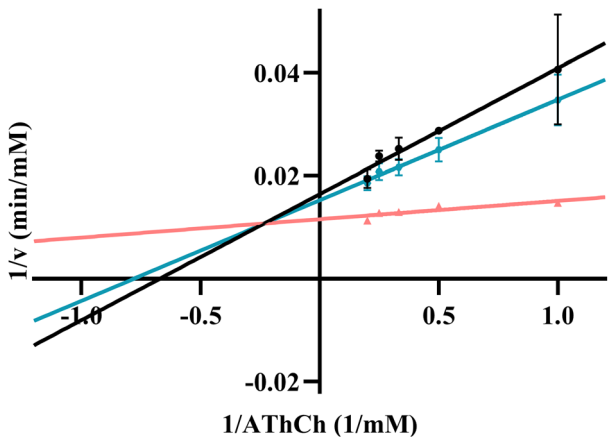

Fig. 9 Lineweaver–Burk plots of RONs immobilized AChE in the presence of huperzine A at different concentrations: (a) 10 μM, (b) 30 μM, (c) 70 μM.

leading to the increased absorbance of the product, ox OPD. The inhibition (IE%) of AChE was used for the analysis of huperzine A. With an increase in huperzine A concentration, the decomposition of MnO_2 nanosheets induced by TCh decreased, resulting in an increase in product absorbance. Under optimal conditions, the inhibition curve was obtained from IE (%) against the logarithm of huperzine A concentration in the range from 0.01 to 100 μM and the IC_{50} value (half-maximal inhibitory concentration) was calculated to be 14.03 μM (Fig. 10).

3.4. AChE inhibitor screening from *Inula macrophylla*

The established RONs immobilized AChE combined with the MnO_2–OPD colorimetric method (RONs immobilized AChE MnO_2–OPD system) was applied to the screening of AChE inhibitors from *Inula macrophylla*. Firstly, the inhibitory effect of the ethyl acetate fraction on AChE was evaluated, and the inhibition was 23.2% at a concentration of 1 mg mL^{-1}. Subsequently, the AChE inhibitory activities of fractions A, B, C, D and E obtained from the gradient elution of ethyl acetate fractions were evaluated, and exhibited 40.0%, 44.0%, 47.0%, 39.2% and 38.4% inhibitions at a final concentration of 1 mg mL^{-1}. Among the five fractions, fraction B and fraction C had strong inhibitory activity against AChE. According to the above method, 14 compounds, isolated from fractions B and C, were screened as enzyme inhibitors. The inhibitory effects of the 14 compounds were measured and are listed in Table 1.

This journal is © The Royal Society of Chemistry 2023

Open Access Article. Published on 11 2566. Downloaded on 24/7/2567 16:33:59.
This article is licensed under a Creative Commons Attribution-NonCommercial 3.0 Unported Licence.

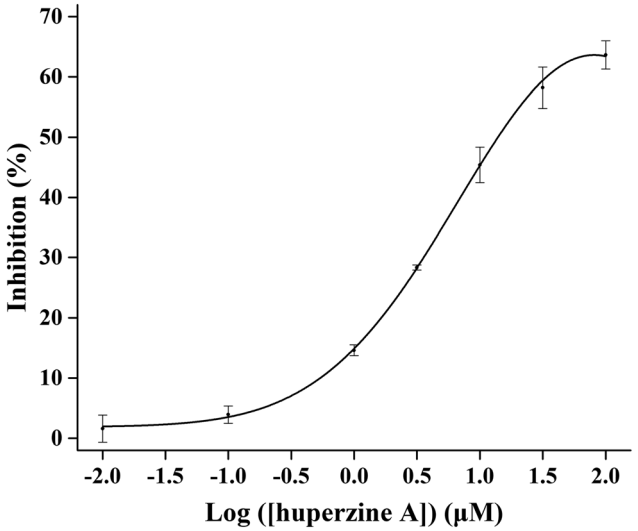

Fig. 10 The inhibition curve for huperzine A on RONs immobilized AChE.

Table 1 Screening AChE inhibitors from 14 compounds from *Inula macrophylla*

Compound	Inhibition (%)	Compound	Inhibition (%)
1	21.1^{a} 14.4^{b}	**8**	61.3^{a} 36.4^{b}
2	42.0^{a} 33.7^{b}	**9**	32.2^{a} 9.2^{b}
3	45.7^{a} 44.2^{b}	**10**	14.1^{a} 8.6^{b}
4	67.9^{a} 64.2^{b}	**11**	73.8^{a} 46.8^{b}
5	69.2^{a} 51.3^{b}	**12**	42.5^{a} 38.6^{b}
6	61.3^{a} 36.5^{b}	**13**	51.1^{a} 31.3^{b}
7	46.9^{a} 37.3^{b}	**14**	66.4^{a} 43.5^{b}

^{a} 0.5 mg mL^{-1}. ^{b} 0.1 mg mL^{-1}.

The results showed that compounds **1**, **9** and **10** had weak inhibitory effects on AChE and could not be used as AChE inhibitors. Compounds **4**, **5**, **11** and **14** had strong inhibitory effects on AChE. At a concentration of 0.5 mg mL^{-1}, the inhibitions were 67.9%, 69.2%, 73.8% and 66.4%, respectively. In a comprehensive evaluation, β-cyclocostunolide (compound **4**) showed the strongest inhibitory effect; even at a concentration of 0.1 mg mL^{-1}, the inhibition was 64.2%. The reduction of the concentration from 0.5 mg mL^{-1} to 0.1 mg mL^{-1} did not greatly reduce the AChE inhibition rate, indicating that β-cyclocostunolide (compound **4**) may be a potential AChE inhibitor. The above screening results showed that the RONs immobilized AChE–MnO_2–OPD system is feasible for the field of inhibitor screening, and also opens up new ideas for the application of nanozymes.

4. Conclusion

In this work, ruptured organosilica nanocapsules (RONs) were employed as a support to immobilize AChE. The cracks and openings on the surface of RONs can promote the immobilization of AChE on the inner wall and surface of RONs through electrostatic interaction. A platform for monitoring AChE activity was constructed by combining the established RONs immobilized AChE with the MnO_2–OPD colorimetric method and quantifying the absorption peak of the product ox OPD at 420 nm by using capillary electrophoresis. The inhibition kinetics showed that the established strategy of RONsimmobilized AChE combined with MnO_2–OPD colorimetry was feasible in the field of AChE inhibitor screening. The new technology of an immobilized enzyme combined with nanozyme was applied to the rapid screening of AChE inhibitors in *Inula macrophylla*, and it was found that β-cyclocostunolide (compound **4**) had strong AChE inhibitory activity. Therefore, this work not only confirms the existence of chemical components that inhibit AChE activity in *Inula macrophylla*, but also lays a foundation for the discovery of AChE inhibitors in *Inula macrophylla* in the future.

Conflicts of interest

The authors declare that they have no known competing financial interests or personal relationships that could have appeared to influence the work reported in this paper.

Acknowledgements

This work was financially supported by the National Key Research and Development Project of China (No. 2021YFE0103700) and the National Natural Science Foundation of China (No. 21974145).

References

1 P. Kasa, *Nature*, 1968, **218**, 1265–1267.
2 R. M. Lane, S. G. Potkin and A. Enz, *Int. J. Neuropsychopharmacol.*, 2006, **9**, 101–124.
3 W. D. Reid, D. R. Haubrich and G. Krishna, *Anal. Biochem.*, 1971, **42**, 390–397.
4 A. Kumar, A. Singh and Ekavali, *Pharmacol. Rep.*, 2015, **67**, 195–203.
5 M. Prince, A. Wimo, M. Guerchet, G. Ali, Y. Wu and M. Prina, *Alzheimer's Disease International, ADI*, London, 2015. Accessed date: August 2015.
6 L. P. Tamara, L. Andreja, M. Tatjana, P. Sandra and V. Vesna, *Curr. Med. Chem.*, 2017, **24**, 3283–3309.
7 S. K. Pandey, U. Yadava, A. Upadhyay and M. L. Sharma, *Bioorg. Med. Chem.*, 2015, **23**, 1135–1148.
8 G. T. Grossberg and A. K. Desai, *J. Gerontol., Ser. A*, 2003, **58**, 331–353.
9 J. L. Yang, N. Z. Song, X. J. Lv and Q. Jia, *Sens. Actuators, B*, 2018, **259**, 226–232.
10 Q. Wang, Z. Nie, Y. F. Hu and S. Z. Yao, *Acta Chim. Sin.*, 2017, **75**, 1109–1114.

Open Access Article. Published on 11 2566. Downloaded on 24/7/2567 16:33:59.
This article is licensed under a Creative Commons Attribution-NonCommercial 3.0 Unported Licence.

11 C. Ye, M. Q. Wang, X. Zhong, S. H. Chen, Y. Q. Chai and R. Yuan, *Biosens. Bioelectron.*, 2016, **79**, 34–40.
12 D. N. Kramer and R. M. Gamson, *Anal. Chem.*, 1958, **30**, 251–254.
13 P. J. Ni, Y. J. Sun, H. C. Dai, S. Jiang, W. D. Lu, Y. L. Wang, Z. Li and Z. Li, *Sens. Actuators, B*, 2016, **226**, 104–109.
14 L. Cheng, F. X. Wu, H. B. Bao, F. H. Li, G. B. Xu, Y. J. Zhang and W. X. Niu, *Small*, 2021, **17**, 2104083.
15 L. J. Su, Y. H. Xiong, H. G. Yang, P. Zhang and F. G. Ye, *J. Mater. Chem. B*, 2016, **4**, 128–134.
16 X. X. Zheng, Q. Liu, C. Jing, Y. Li, D. Li, W. J. Luo, Y. Q. Wen, Y. He, Q. Huang, Y. T. Long and C. H. Fan, *Angew. Chem., Int. Ed.*, 2011, **50**, 11994–11998.
17 L. Li, L. Zhang, U. Carmona and M. Knez, *Chem. Commun.*, 2014, **50**, 8021–8023.
18 X. Cao and N. Wang, *Analyst*, 2011, **136**, 4241–4246.
19 Y. Wan, P. Qi, D. Zhang, J. J. Wu and Y. Wang, *Biosens. Bioelectron.*, 2012, **33**, 69–74.
20 J. J. X. Wu, X. Y. Wang, Q. Wang, Z. P. Lou, S. R. Li, Y. Y. Zhu, L. Qin and H. Wei, *Chem. Soc. Rev.*, 2019, **48**, 1004–1076.
21 J. Liu, L. J. Meng, Z. F. Fei, P. J. Dyson, X. N. Jing and X. Liu, *Biosens. Bioelectron.*, 2017, **90**, 69–74.
22 K. Kai, Y. Yoshida, H. Kageyama, G. Saito, T. Ishigaki, Y. Furukawa and J. Kawamata, *J. Am. Chem. Soc.*, 2008, **130**, 15938–15943.
23 J. H. Wu, Q. T. Yang, Q. Li, H. Y. Li and F. Li, *Anal. Chem.*, 2021, **93**, 4084–4091.
24 R. R. Deng, X. J. Xie, M. Vendrell, Y. T. Chang and X. G. Liu, *J. Am. Chem. Soc.*, 2011, **133**, 20168–20171.
25 A. A. Caparco, D. R. Dautel and J. A. Champion, *Small*, 2022, **18**, 21064.
26 J. N. Wang, M. Y. Bao, T. X. Wei, Z. Y. Wang and Z. H. Dai, *Anal. Chim. Acta*, 2020, **1098**, 148–154.
27 J. Kraly, M. A. Fazal, R. M. Schoenherr, R. Bonn, M. M. Harwood, E. Turner, M. Jones and N. J. Dovichi, *Anal. Chem.*, 2006, **78**, 4097–4110.
28 V. Kostal, J. Katzenmeyer and E. A. Arriaga, *Anal. Chem.*, 2008, **80**, 4533–4550.
29 J. Gao, W. X. Kong, L. Y. Zhou, Y. He, L. Ma, Y. Wang, L. Y. Yin and Y. J. Jiang, *Chem. Eng. J.*, 2017, **309**, 70–79.
30 F. P. Chang, Y. Hung, J. H. Chang, C. H. Lin and C. Y. Mou, *ACS Appl. Mater. Interfaces*, 2014, **6**, 6883–6890.
31 Y. Jiang, L. Shi, Y. Huang, J. Gao, X. Zhang and L. Zhou, *ACS Appl. Mater. Interfaces*, 2014, **6**, 2622–2628.
32 M. R. Correro, N. Moridi, H. Schützinger, S. Sykora, E. M. Amman, E. H. Peters, Y. Dudal, P. F. X. Corvini and P. Shahgaldian, *Angew. Chem., Int. Ed.*, 2016, **55**, 6285–6289.
33 H. Lineweaver and D. Burk, *J. Am. Chem. Soc.*, 1934, **56**, 658–666.
34 M. J. C. Ordoñez, K. J. Balkus, J. P. Ferraris and I. H. Musselman, *J. Membr. Sci.*, 2010, **361**, 28–37.
35 U. P. N. Tran, K. K. A. Le and N. T. S. Phan, *ACS Catal.*, 2011, **1**, 120–127.
36 C. H. Kuo, Y. Tang, L. Y. Chou, B. T. Sneed, C. N. Brodsky, Z. P. Zhao and C. K. Tsung, *J. Am. Chem. Soc.*, 2012, **134**, 14345–14348.
37 M. R. Correro, N. Moridi and H. Schîtzinger, *Angew. Chem., Int. Ed.*, 2016, **55**, 6285–6289.
38 R. Deng, X. Xie, M. Vendrell, Y. T. Chang and X. Liu, *J. Am. Chem. Soc.*, 2011, **133**, 20168.
39 L. Z. Gao, J. Zhuang, L. Nie, J. B. Zhang, Y. Zhang, N. Gu, T. H. Wang, J. Feng, D. L. Yang, S. Perrett and X. Y. Yan, *Nat. Nanotechnol.*, 2007, **2**, 577–583.
40 G. Yang, Y. Wang, J. Tian and J. Liu, *PLoS One*, 2013, **8**, e74916.

This journal is © The Royal Society of Chemistry 2023